Treatment of arbitrarily autocorrelated load functions in the scope of parameter identification *

Katrin Runtemund [1] †, Giulio Cottone [2] ‡and Gerhard Müller [1] §

[1] Lehrstuhl für Baumechanik, Technische Universität München,

Arcisstr. 21, D-80333 München, Germany,

[2] Engineering Risk Analysis Group, Technische Universität München,

Theresienstr. 90, building N6, 80290, Germany

Keywords: Spectral Factorization; Gaussian Stationary Noises; Fractional Spectral Moments; Extended Kalman Filter; Parameter identification; Ambient Vibration Tests

Abstract

Ambient vibration tests are output-only tests based on the structural response recorded under natural excitation, such as wind or traffic loads. In contrast to forced vibration test, they do not require service interruption and expensive devices to excite the structure. To this aim, we combine the recently proposed H-fractional spectral moments representation of stationary processes with a modification of the Kalman filter to the scope of structural parameter identification. This paper shows that the method is particularly suited to dealing with long-correlated loads, i.e. stochastic processes with inverse power-law correlation, where many existing methods are not applicable or insufficiently accurate.

1 Introduction

Forced vibration tests on structures of civil engineering interest are expensive and time consuming as they are performed by impact hammers or heavy shakers, needed to excite the modes of interest with sufficient energy. Moreover, they require temporary out of service state of the structure which causes increments of costs. Conversely, ambient vibration test can be conducted continuously in time measuring the structural response for large time intervals, using the excitation of both natural and/or service loads as wind, traffic or human walk. Such loads are caused by the superposition of multiple inputs and thus lead to a broad-band excitation of a significant number of vibration modes [58, 16].

A literature review on ambient vibration tests can be found in [25]. The first use of the ambient vibration technique for the dynamic characterization of full-scale structures is reported in the seventies. Since then the technique is extensively used in engineering in the scope of parameter identification (frequencies, damping ratios and modal shapes) [27, 41, 40, 17, 6, 44, 22], model updating [26, 22] as well as damage detection and health monitoring [20,

*accepted in Computers and Structures

†E-mail: katrin.runtemund@bv.tum.de

‡E-mail: giulio.cottone@tum.de; giuliocottone@yahoo.it

§E-mail: gerhard.mueller@bv.tum.de

42, 33] of slender structures such as pedestrian bridges, chimneys, long-span frame structures or high-rise buildings.

Many experimental modal identification methods for output-only measurements are available if the load process can be modeled as a stochastic white noise process: i) The peak picking method [2, p. 196-203] in which the eigenfrequencies of the system are determined from the resonant peaks of the averaged normalized power spectral densities (ANPSDs) of the system response, is widely used in civil engineering due to its simplicity and computational efficiency. In case of a broad-band excitation, well separated modes and low damping, the method provides reliable estimates of the eigenfrequencies [22]. ii) The stochastic subspace identification method [41, 17] belongs to the most advanced time-domain methods which identifies the system matrices of a stochastic state space model from which the modal parameters can be extracted using numerical techniques such as singular value decomposition (SVD) or QR factorization. The unknown input is introduced as zero-mean white process noise in the system equation. Hence, if the input contains some dominant frequencies, they cannot be distinguished from the eigenvalues of the system matrices used for the parameter identification [44]. iii) The natural excitation technique (NExT) is based on the fact that the theoretical cross-correlation function between two response output channels from an ambient excited structure has the same analytical form as the free vibration response of the structure [27]. Hence, classical modal parameter estimation techniques such as Polyreference, LSCE, Eigensystem Realization Algorithm (ERA) and Ibrahim Time Domain are appropriate to estimate the modal parameters using the cross-correlation function instead of the impulse response function as input [40]. A comparative study on these system identification techniques is given in [17, 40]. In case the power spectral density (PSD) of the excitation is not white, the above cited methods are not applicable. In this case, the parameter identification problem to be solved consists of two subparts, namely: i) The digital simulation of the random load; ii) The estimation of the structural response to the random load using output-only model identification techniques. In case that both parts are handled individually, numerous methods for the system identification as well as for the simulation of stochastic processes are available. To better motivate the method proposed in this paper we briefly review some methods appeared in literature to handle both problems.

1.1 Digital simulation of stationary Gaussian processes

A literature review on different simulation techniques of stationary Gaussian processes with application to wind engineering was proposed in [32]: They are classified in spectral representation approaches and digital filter schemes with band-limited white noise input. The first class is based on the superposition of (a theoretical infinite) series of sine and cosine functions with random phase either carried out in the time or in the frequency domain using fast Fourier transform (FFT) [57] and was proposed in the seventies by [50]. It belongs to the most popular methods for the digital simulation of random processes and allows to generate sample functions with target probabilistic characteristics of stationary/ non-stationary, homogeneous/non-homogeneous, one-dimensional/multi-dimensional, one-variate/multi-variate as well as Gaussian/ non-Gaussian stochastic processes, fields or waves. Combined with the Monte Carlo Simulation algorithm, the method can be applied to a variety of engineering problems in stochastic mechanics such as nonlinear problems or problems related to the stochastic stability, parametric excitation, parameter and input uncertainties, risk assessment, etc.. However, especially if processes with a large number of variates are considered, computational difficulties arise. The use of the Fast Fourier transform improves the computational efficiency drastically, but not without the expense of increased demand on computer storage [32]. Even in the case of one-dimensional univariate stochastic processes the generation of samples might be extremely expensive from a computational point of view, if the generation is to be performed

over a long period of time [48]. However, the crucial problem arises from the fact, that the obtained series representation of the process cannot be written in the required state space form in order to combine it with the later used system identification technique. A similar problem occurs if the Karhunen-Loéve decomposition of the random process is used. This is based on linear superposition of deterministic functions where the combination factors are a set of uncorrelated random variables [35, p. 27 ff.]. Also in this approach the resulting equations cannot be written in state space form and hence the method is not appropriate.

In the second class of simulation techniques, the process is modeled as output of a linear system subjected to white noise represented either by convolution of the input process with the impulse response function or by integration of a differential equation driven by white noise. The former is based on the spectral factorization theorem and the latter leads to parametric time series models such as autoregressive (AR), moving average (MA), and the combined ARMA models to simulate the time series of the random process. The linear model describing the load process can then be included in the structural state representation of the system's dynamics by state space augmentation to which standard tools based on linear system theory for the system identification as considered here, but also in the scope of response analysis, optimization, and design of active control devices, can be applied [9].

Moving average models are widely used for the simulation of random processes characterized by an all-zero spectra, i.e. if the estimated PSD has no prominent peaks, in contrast to autoregressive models which are more suitable for all-pole spectra, i.e. if the PSD is characterized mainly by spectral peaks at distinct frequencies.

Their combination, the ARMA model, yields a PSD with peaks and expressible as ratio of polynomials [51, 5, 31] suitable for a wide range of spectra with both poles and zeros. While the coefficients of the AR model can be derived by linear regression, the approximation of the process by the more general ARMA model leads to a highly non-linear minimization problem. In [52, 38, 54, 55] the optimization problem is solved by two stage algorithms where first the process is approximated as high order AR series by autocorrelation matching and then in a second step a low order ARMA representation of the prior model is derived by matching of the output autocorrelations and input-output cross-correlations. The methods are verified by application to spectra encountered in earthquake engineering (Kanai-Tajimi spectrum), wind engineering (von Kármán velocity spectrum) and ocean engineering (Pierson-Moskowitz (P-M) spectrum). However, the methods require a repetitive calculation of the AR and ARMA parameters in order to find the optimal order of these models. At the best of the authors' knowledge, there are not methods to a priori estimate the number of coefficients to be calculated for the AR and MA parts. In case that the target spectrum exhibits zeros like the P-M spectrum or a slope discontinuity like the Davenport spectrum, the computation of reliable AR approximations need some further tuning of the ARMA model [37]. Zeros in the target spectrum leads indeed to high frequency fluctuation in the corresponding AR spectrum whose amplitude decays slowly with increasing system order. The problem is discussed in detail in scope of the properties of the z-Transform in [52], where a Taylor series expansion of the P-M spectrum is proposed to reduce the effect of the zero in the spectrum. Instead of approximating the ARMA representation on basis of a high order AR model in [53] the problem is solved by a two stage approach, where the first step is to calculate a high order MA representation being more suited to model zeros is the spectrum. In [37] it is shown that the rate of convergence of this algorithm can be improved by adding a very small positive value to the target spectrum so that the zero, causing the numerical problems, is removed. Slope discontinuities in the spectrum also lead to a slow convergence of the AR model to the target process, in particular a kink at small frequency leads to a decrease of the converges rate. The AC function $R(\tau)$ of ARMA generated processes converges exponentially as the lag $\tau \to \infty$, and thus are just applicable for the description of short-memory processes. Long-memory processes are characterized by a much slower decreasing AC function, i.e. $R(\tau) \sim C\tau^d$ as

$\tau \to \infty$ where $C > 0$ and $-2 < d < 0$, and can be described by a modified form, the so-called fractionally integrated ARMA processes (ARFIMA) proposed in [23] which can be interpreted as ARMA processes driven by fractionally integrated white noise [4, p. 428–436]. Since the AC function decays slowly, the estimation of the model parameters, e.g. by applying the maximum likelihood procedure, requires the consideration of all autocorrelations including those with large time lags what makes the method computational demanding. As the state space representation of an ARFIMA model is of infinite order [8] it is not computationally efficient when combined to algorithms for system identification. Further literature on techniques for the generation of time series with power law PSDs such as fractional integration-based methods, fractional Brownian motion method, Fourier transform based-methods, wavelet-based methods and methods based on ARMA filters is given in [21].

1.2 Parameter identification for structures under correlated loads

In case of non-white excitation, the parameter identification problem is more complex and few techniques appeared in literature. In [19, 18] an operational modal analysis technique on transmissibility measurements is introduced which allows to identify the modal parameters of the structure without assumption on the nature of the excitation. In [43] a multi-dimensional ARMA parameter identification method is derived which allows to consider the excitation by sinusoidal loads, non-stationary white noise as well as colored noise with a rational spectrum. The latter property is also used in [34] where the state space model is augmented for correlated process noise using the spectral factorization theorem. It allows to model a wide sense stationary random process with PSD of rational form as an output of a linear system with white noise input. This system is then added to the original system by augmenting the state space representation leading to an overall linear system driven by white noise once again. The parameter identification is then carried out with the help of the extended Kalman filter (EKF) [34], a modification of the well-known Kalman filter [30] that is a minimum variance parameter estimator.

1.3 Motivations and aim of the paper

From the literature review it can be summarized that at the state-of-the-art, the main limitations in the field of parameter identification under correlated loads are: i) if the load is long-correlated, time series models require an infinite number of coefficients to properly simulate the inverse power-law decay; ii) the number of coefficients p and q of time series models, such as ARMA models, cannot be predicted a priori and, increasing them, requires the recalculation of the whole set of coefficients; iii) this limitation is more severe from the computational time point of view in multivariate and multidimensional cases; iv) efficient simulation methods, based on Karhunen-Loéve or wavelet methods, have not been yet combined to identification methods.

The problem which is addressed in this paper is the development of a method for the digital simulation of random forces from the knowledge of the PSD which can be easily combined with existing identification methods, solving the issues above summarized.

The problem is solved on basis of a recently developed method which allows to represent PSD and correlation function (AC) in closed form by means of a generalized Taylor expansion using fractional spectral moments (FSMs) [11]. The concept is used in [15] to derive a linear fractional differential equation, whose output is a stationary colored Gaussian process with target PSD, e.g. known from measurements. The method is called 'H-fractional spectral moments decomposition' as the coefficients for the noise simulation are calculated from the

FSMs of the linear transfer function $H(\omega)$. In [10, 13] it is applied for the simulation of univariate/multivariate wind velocity fields, respectively. Based on the H-FSMs decomposition the new issue presented in this paper is the derivation of a state space representation of arbitrarily correlated load processes in analytical form which neither require the factorization of the PSD nor any optimization procedure and which can be easily combined with common state space model based system identification methods such as the well known and widely used Kalman filter algorithm.

In the following, the H-FSM method is described and some relevant applications in wind and ocean engineering are presented. Then, the Kalman filter algorithm is introduced and modified in order to include time-correlated process noise by state space augmentation. Here we will follow an approach given in [34] which uses the spectral factorization theorem for this purpose. The method is introduced for the validation of the developed generalized state space representation. Finally, the fractional algorithm is applied to a single degree of freedom system excited by the three load cases in order to estimate the stiffness and damping parameter of the system.

2 Fractional representation of stationary Gaussian processes

In the following we present a method to describe a stationary colored Gaussian process as output of a linear fractional differential equations, recently introduced in [15].

A colored Gaussian noise process $F(t)$ can be represented as output of a linear differential equation, a so-called linear filter, excited by a Gaussian white noise process $\{W(t)\}$. The input-output relation is characterized in the frequency domain by the transfer function $H(\omega)$ [36]. Many methods exist to find $H(\omega)$ given the target PSD of $\{F(t)\}$, with the aim of simulating realizations of the process $\{F(t)\}$. Stationary Gaussian processes $\{X(t)\}$, which will be considered in the following, are completely characterized by the second order statistics, i.e. the first and second order moments, namely the mean $\mu(t)$ and AC function $R(\tau)$

$$\mu(t) = E\left[X(t)\right] = const. \tag{1a}$$

$$R_X(\tau) = \int_{-\infty}^{\infty} X(t)X(t+\tau)\mathrm{d}\tau = E\left[X(t)X(t+\tau)\right] \tag{1b}$$

where $E[\,\cdot\,]$ denotes the stochastic average and τ an arbitrary time shift. Alternatively, the process can be characterized in the frequency domain by its PSD $S_X(\omega)$, e.g. known from measurements. The AC and the PSD are related by the Fourier transform pair

$$R_X(\tau) = \mathcal{F}\{S_X(\omega); t\} = \int_{-\infty}^{\infty} S_X(\omega)e^{i\omega\tau}\mathrm{d}\omega \tag{2a}$$

$$S_X(\omega) = \mathcal{F}^{-1}\{R_X(\tau); \omega\} = \frac{1}{2\pi}\int_{-\infty}^{\infty} R_X(\tau)e^{-i\omega\tau}\mathrm{d}\tau \tag{2b}$$

As shown in [11] both the AC and the PSD function can be reconstructed by fractional spectral moments (FSMs) defined as

$$\Lambda_X(\gamma) = \int_{-\infty}^{\infty} |\omega|^{\gamma} S_X(\omega)\mathrm{d}\omega = \int_{0}^{\infty} \omega^{\gamma} G_X(\omega)\mathrm{d}\omega \tag{3}$$

with $\gamma \in \mathbb{C}$ chosen such that the integral converge, that is with the real part $\gamma_0 < Re\gamma < \gamma_1$.

For $\gamma \in \mathbb{N}_{>0}$ the FSMs coincide with the classical spectral moments (SMs) of the one-sided PSD function $G_X(\omega) = 2U(\omega)S_X(\omega)$ already defined in [56] where $U(\omega)$ is the unit step function. In particular the zero-order SM $\Lambda_X(\gamma = 0)$ corresponds to the variance of the process $\{X(t)\}$ and the second-order SM $\Lambda_X(\gamma = 2)$ is the variance of its derivative $\{\dot{X}(t)\}$. While the classical SMs might diverge if γ increases and thus cannot be used to reconstruct the PSD of the process, it was proven, in [12], that for $\gamma \in \mathbb{C}$ the FSMs $\Lambda_X(\gamma)$ restore both the $R_X(\tau)$ and $S_X(\omega)$ in the form

$$R_X(\tau) = \frac{1}{2\pi \mathrm{i}} \int_{\rho-\mathrm{i}\infty}^{\rho+\mathrm{i}\infty} \nu(\gamma)\Lambda_X(-\gamma)|t|^{-\gamma}\mathrm{d}\gamma \tag{4a}$$

$$S_X(\omega) = \frac{1}{4\pi \mathrm{i}} \int_{\rho-\mathrm{i}\infty}^{\rho+\mathrm{i}\infty} \Lambda_X(-\gamma)|\omega|^{\gamma-1}\mathrm{d}\gamma \tag{4b}$$

where $\nu(\gamma) = \Gamma(\gamma)\cos(\gamma\pi/2)$ and $\gamma_0 < \rho < \gamma_1$. Both integrals are performed along the imaginary axis with fixed real part ρ which belongs to the fundamental strip of the Mellin transform calculated from Eq.(3). Furthermore in deriving the latter equation it was considered that the AC, and consequently the PSD, are symmetric and real functions. This representation is valid for any Fourier pair, originally was proposed for probability density and characteristic function in [12], and extended to multidimensional random variables [14] and multivariate processes [10, 13].

In contrast to the methods based on time series, such as the ARMA-based methods, the coefficients of the model are derived in analytical form and allow to formulate a representation of both the PSD and AC function in the whole domains $]-\infty < \omega < \infty[$ and $]-\infty < \tau < \infty[$, respectively. The method can be used for arbitrarily correlated processes with no requirement to the functional form of the PSD, and thus it allows to model both short- and long-memory dependencies. Furthermore, it must be noted, that the coefficients are calculated analytically directly on basis of the target PSD function instead of the AC function like the ARMA-based approaches which makes the method computational efficient also in case of long correlated processes. In the second part, it will be shown, that once the coefficients of the process are calculated, the algorithm can be readily expressed as linear state space form with white noise input which allows to combine it with the used identification algorithm.

2.1 Reconstruction of the PSD of correlated Gaussian processes by H-FSMs decomposition

In the following the main results of the method for the representation of colored Gaussian processes described in [15] are summarized for clarity's sake. Three load case scenarios, i.e. process with exponential AC, von Kármán and Pierson Moskowitz PSD, are examined which are used throughout the paper for verification of the method.
Using this method the colored load process $\{F(t)\}$ with assigned PSD $S_F(\omega)$ is simulated as output of a linear differential equation excited by Gaussian white noise. This can be expressed using the linear differential operator $\mathcal{L}(\cdot)$ in the form

$$\mathcal{L}(F(t)) = W(t) \tag{5}$$

where $\{W(t)\}$ denotes the zero-mean Gaussian white noise process. The corresponding input-output relation in terms of the PSD are given by

$$S_F(\omega) = |H(\omega)|^2 S_W(\omega) \tag{6}$$

where $H(\omega)$ is the transfer function and $S_W(\omega)$ denotes the PSD of the zero-mean Gaussian white noise process $\{W(t)\}$ of intensity q_W characterized by the Fourier pair

$$S_W(\omega) = \frac{q_W}{2\pi} R(\tau) = E[W(t)W(t+\tau)] = q_W\, \delta(\tau). \tag{7}$$

Assuming

$$Arg[H(\omega)] = 0 \tag{8}$$

the filter is defined from the target PSD

$$H(\omega) = |H(\omega)| = \sqrt{\frac{2\pi}{q_W} S_F(\omega)} \tag{9}$$

In the time domain, the solution of Eq.(5) is given by the Duhamel convolution integral

$$F(t) = \int_{-\infty}^{\infty} h(t-\tau) W(\tau) \mathrm{d}\tau = \int_{-\infty}^{\infty} h(\tau) W(t-\tau) \mathrm{d}\tau. \tag{10}$$

using the time-invariant linear transfer function $h(t) = \mathcal{F}\{H(\omega); t\}$. It must be noted that the assumption Eq.(8) leads to a non-causal system, i.e. $h(t) \neq 0$ for $t < 0$, hence, the generated time series of the process $\{F(t)\}$ is not just depending on the realizations $W(t_0), W(t_{-1}), W(t_{-2}), ...$ of the white noise process $\{W(t)\}$ for $t < 0$ but also on future values $W(t_1), W(t_2), ...$ for $t > 0$. Nevertheless, due to the linearity of the underlying differential equation and the statistical independence of the Gaussian white noise process, the output remains a strict stationary Gaussian process. In order to reconstruct the transfer function $H(\omega)$ and its Fourier transform one can follow the approach derived in the previous section for the AC function and PSD leading to the H-fractional spectral moments (H-FSM)

$$\Pi_H(\gamma) = \int_{-\infty}^{\infty} H(\omega)\, |\omega|^{\gamma}\, \mathrm{d}\omega \tag{11}$$

as shown in [11]. Similar to Eq.(4a), (4b) the transfer function $h(t)$ and its Fourier transform $H(\omega)$ can be represented by

$$h(t) = \frac{1}{2\pi i} \int_{\rho - i\infty}^{\rho + i\infty} \nu(\gamma) \Pi_H(-\gamma)\, |t|^{-\gamma}\, \mathrm{d}\gamma \tag{12a}$$

$$H(\omega) = \frac{1}{4\pi i} \int_{\rho - i\infty}^{\rho + i\infty} \Pi_H(-\gamma)\, |\omega|^{\gamma - 1}\, \mathrm{d}\gamma \tag{12b}$$

with $\nu(\gamma) = \Gamma(\gamma) \cos(\gamma\pi/2)$. In some cases these contour integrals cannot be calculated in analytical form, but as the Gamma function $\Gamma(\gamma)$ decays exponentially fast in vertical strips, i.e. for $Im\gamma \to \infty$, depending on the decay of $\Pi_H(\gamma)$, the integrals might be truncated along the imaginary axis with constant real part $Re\gamma = \rho$ and approximated by their sums

$$h(t) \approx \frac{\Delta\eta}{2\pi} \sum_{k=-m}^{m} \nu(\gamma_k) \Pi_H(-\gamma_k)\, |t|^{-\gamma_k} \tag{13a}$$

$$H(\omega) \approx \frac{\Delta\eta}{4\pi} \sum_{k=-m}^{m} \Pi_H(-\gamma_k)\, |\omega|^{\gamma_k - 1} \tag{13b}$$

Defining $\gamma_k = \rho + \mathrm{i}k\Delta\eta$, the integral is calculated up to a certain value $\bar{\eta} = \mp m\Delta\eta$ by discretizing the interval into $2m + 1$ small increments $\Delta\eta$.

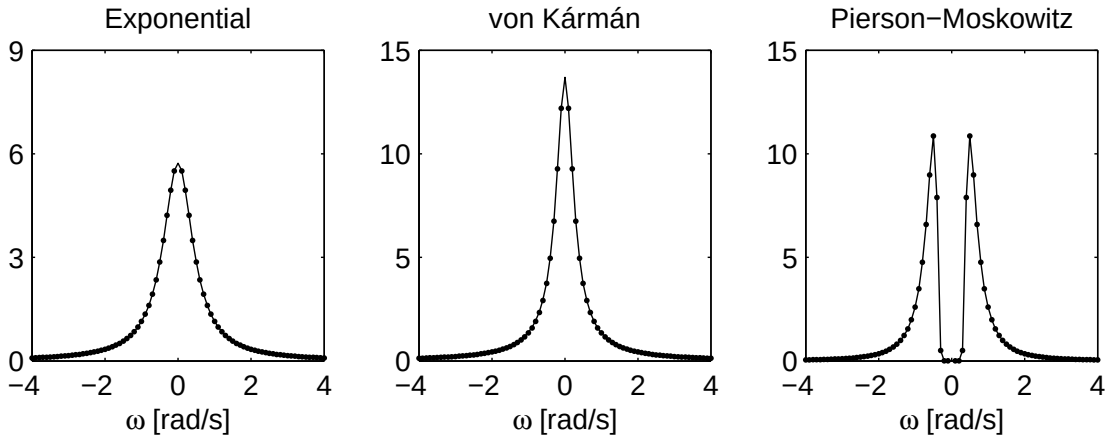

Figure 1: Exact (continuous) and approximated (dotted) power spectral densities for the three load cases: exponential AC, von Kármán and P-M PSD

2.1.1 Numerical examples

Three load processes which are widely used in wind and ocean engineering are discussed.

1. Exponentially autocorrelated wind gusts
The most simplest model for the description of along wind turbulences is a process with exponential AC function $R(\tau) = \sigma^2 e^{-a|t|}$ and corresponding rational low-frequency power spectrum $S_F(\omega)$ given by

$$S_F(\omega) = \frac{a\sigma^2}{\pi(a^2+\omega^2)} \tag{14}$$

The H-FSMs of the transfer function $H(\omega) = \sqrt{2\pi S_F(\omega)/q}$ in Eq.(9) can be easily calculated by Mathematica using Eq.(11) and are given by

$$\Pi_H(\gamma) = \left(\frac{1}{a^2}\right)^{-\gamma/2} \sqrt{\frac{2a\sigma^2}{q\pi}} \Gamma\left(-\frac{\gamma}{2}\right) \Gamma\left(\frac{1+\gamma}{2}\right); \qquad -1 < Re\gamma < 0 \tag{15}$$

The PSD $S_F(\omega)$ of the process is reconstructed by the relation $S_F(\omega) = |H(\omega)|^2 q/(2\pi)$. The approximation of the transfer function $H(\omega)$ in Eq.(13b) is calculated choosing $a = 0.5$ [1/s], $\sigma = 3$ [N] and $\rho = 0.6$, $\Delta\eta = 0.2$ for the discretization of the integral involved taking into account $m = 20$ FSMs. From the results depicted in Fig.(1) it can be stressed that the proposed reconstruction leads to a good approximation of the analytic PSD. Moreover, the quality of the approximation depends solely on the chosen discretization of the integral given in Eq.(13b).

2. Wind gusts with von Kármán velocity PSD
In general, if the PSD is rational it is not difficult to find a transfer function by spectral factorization [36, p. 180–195]. However, if the PSD of the process noise is given by a not rational function, there is no general method available for the analytically derivation of the transfer function $H(s)$ by spectral factorization and this is in fact a nontrivial task [1]. This is the case for the widely used von Kármán spectrum of along-wind turbulences given by

$$S_{Kar}(\omega) = \frac{\sigma^2 L}{\pi \bar{u}_z} \frac{1 + \frac{8}{3}\left(1.339 L \frac{\omega}{\bar{u}_z}\right)^2}{\left[1 + \left(1.339 L \frac{\omega}{\bar{u}_z}\right)^2\right]^{11/6}} \tag{16}$$

where σ, L is the standard deviation of the fluctuating component of the wind speed at height z and the integral turbulence scale lengths, respectively, and $\bar{u}_z$ denotes the mean velocity with

which the assumed frozen-turbulence field propagates in space (Taylor's frozen-in turbulence hypothesis [24]). The PSD of the corresponding wind load is given by

$$S_F(\omega) = (\rho_a C_d A \bar{u}_z)^2 \left|\chi_a(z,\omega)\right|^2 S_{Kar}(\omega) \qquad \chi_a(z,\omega) = \left[1 + \left(\frac{2\omega\sqrt{A}}{\bar{u}_z}\right)^{4/3}\right]^{-1} \tag{17}$$

using the aerodynamic admittance $\chi_a(z,\omega)$ [46, 47] and where ρ_a denotes the air density, C_d the drag coefficient, A the projected area of the structure and $\bar{u}(z)$ is the mean wind speed at height z. Numerical values for the parameters for Germany can be taken e.g. from the national annexe of the "Eurocode 1: Actions on structures, Part 1-4: General actions/Wind actions" (DIN EN 1991-1-4:2010-12). In the example the parameters were chosen arbitrarily: $L = 10$ [m], $\sigma = 1$ [m/s], $z = 3$ [m], $\bar{u}_z = 18.25$ [m/s], $C_D = 1$ [-], $A = 0.1$ [m^2] and $\rho_a = 1.25$ [kg/m^3]. The transfer function $H(\omega)$ is calculated by introducing Eq.(17) into Eq.(9) and the associated H-FSMs follow from Eq.(11) using Mathematica. This leads to

$$\Pi_H(\gamma) = C(\gamma) + \sum_{k=0}^{2} \frac{D\Gamma[\frac{5+2c_k}{12}]\Gamma[\frac{-1}{6c_k}]{}_3F_2[1, \frac{2c_k+5}{24}, \frac{2c_k+17}{24}; \frac{c_k+6}{12}, \frac{c_k+12}{12}, \frac{-b^2L^4}{A^2}]\bar{u}_z^{\frac{3}{2}+\gamma}}{(-1)^k b^{\frac{-1}{6c_k}} \bar{A}^{\frac{2(1+k)}{3}} L^{\frac{-c_k}{3}} \Gamma[\frac{5}{12}]} \tag{18}$$

for $-1 < Re\gamma < 7/6$ with

$$C(\gamma) = -\frac{3i\pi D \bar{A}^{-\frac{1+\gamma}{2}} e^{\frac{3i\pi(1+\gamma)}{4}} (-ie^{\frac{3i\pi\gamma}{2}}(1 - \frac{ibL^2}{\bar{A}})^{\frac{5}{12}} + (1 + \frac{ibL^2}{\bar{A}})^{\frac{5}{12}})\bar{u}_z^{\frac{3}{2}+\gamma}}{(1 + e^{3i\pi\gamma})(1 + \frac{b^2L^4}{\bar{A}^2})^{\frac{5}{12}}} \tag{19}$$

where $c_k = 1+4k-3\gamma$, $b = 70.8$, $\bar{A} = 4A$, $D = \sqrt{8\pi L(AC_d\sigma\rho_a)^2/q}$ and ${}_pF_q[a_1, ...a_p; b_1, ...b_q; z]$ is the generalized hypergeometric function. The analytical form of the H-FSMs leads, also in this case, to a very efficient application of the method. In Fig.(1) the results are illustrated having chosen the following parameters: $\rho = 0.6$, $\Delta\eta = 0.15$, $m = 30$.

3. Wind waves with Pierson Moskowitz PSD

In this last example the process noise is generated from a wind wave PSD of fully developed sea introduced by Pierson and Moskowitz (P-M). It was developed on the basis of 460 spectra obtained from measurements in the North Atlantic Ocean from 1955 to 1960 and is given by

$$S_{PM}(\omega) = \frac{a}{\omega^5} e^{-\frac{b}{\omega^4}} \tag{20}$$

where $a = 0.0081g^2$, $b = 0.74(g/\bar{u}_{19.5})^4$, g is the acceleration due to gravity and $\bar{u}_{19.5}$ denotes the mean velocity at height $z = 19.5$ [m] above the sea surface. Assuming a stationary process the wave force acting on a vertical pile with diameter D at height z is given by

$$S_F(z,\omega) = \left(\frac{8}{\pi}\sigma_u^2 K_d^2 + K_1^2\omega^2\right)\left(\frac{\omega\cosh(k(z+h))}{\sinh(kh)}\right)^2 S_{PM}(\omega) \tag{21}$$

with $K_d = 1/2\rho_w C_d D$, $K_1 = \rho_w C_m \pi D^2/4$ and where k is the angular wave number, h the water depth, ρ_w is the density of the sea water, C_m is the inertia coefficient and σ_u is the standard deviation of the fluid particle velocity [35]. In general C_m ranges between $1.6 - 2.5$ and for a vertical cylinder $C_m = 2.0$ can be assumed. The drag coefficient C_d never falls below 0.6 and for a smooth cylinder $C_d = 1.0$ [39]. Eq.(21) is valid for non-breaking waves and when the dimension of the structure is small compared to the wave length λ, i.e. when $D < 0.2\lambda$. A detailed description of the derivation of Eq.(21) can be found in [35]. The H-FSMs are given, also in this case, in analytical form

$$\begin{aligned}\Pi_H(\gamma) \quad = \frac{2^{c-2}}{b^{\frac{1}{8}}}\sqrt{\frac{a\cosh[k(h+z)]^2}{Aq\sinh[hk]^2}}\Big(&Ab^{\frac{\gamma}{4}}\sqrt{8\pi}\Gamma[c]{}_2F_2\left[-\tfrac{1}{4}, \tfrac{1}{4}; \tfrac{1}{2}, 1-c, -\frac{bB^2}{2A^2}\right] + \\ &+b^{\frac{5}{8}-c}B\sqrt{\pi}\Gamma\left[c-\tfrac{1}{2}\right]{}_2F_2\left[\tfrac{1}{4}, \tfrac{3}{4}; \tfrac{3}{2}, \tfrac{3}{2}-c; -\frac{bB^2}{2A^2}\right] + \\ &-2^{\frac{3}{2}-c}b^{\frac{1}{8}}A^{1-2c}B^{2c}\,\Gamma\left[2c-\tfrac{1}{2}\right]\Gamma[-2c]{}_2F_2\left[c-\tfrac{1}{4}, c+\tfrac{1}{4}; c+\tfrac{1}{2}, c+1; -\frac{bB^2}{2A^2}\right]\Big)\end{aligned}$$

for $Re\gamma < -1/2$ and $c = 1/8 - \gamma/4$, A=$8/\pi\sigma_u^2 K_d^2$ and $B = K_1^2$. In the example a pile with diameter $D = 0.1$ [m], drag coefficient $C_d = 0.6$ [-] and inertia coefficient $C_m = 2$ [-] which is excited by wind-induced ($\bar{u}_{19.5} = 20$ [m/s], $\sigma_u = 1$ [m/s]) ocean waves with wave length $\lambda = 20$ [m] and water depth $h = 15$ [m] is assumed. The corresponding PSD of the wave loads and the approximation using $m = 40$ FSMs and $\rho = 1.6$, $\Delta\eta = 0.3$ for the discretization of the integral involved is depicted in Fig.(1). Once again a good agreement between the approximated and the exact PSD is obtained.

2.2 Digital simulation of the load process

The obtained fractional representation of the transfer function $H(\omega)$ given in Eq.(12b) can be now introduced in the input-output relation $F_k(\omega, T) = H(\omega)W_k(\omega, T)$

$$F_k(\omega, T) = \frac{1}{4\pi i} \int_{\rho - i\infty}^{\rho + i\infty} \Pi_H(-\gamma)\, |\omega|^{\gamma - 1}\, W_k(\omega, T) d\gamma \tag{22}$$

where $0 < t < T$ and k denotes the index of the ensemble of the process $\{F(t)\}$, $\{W(t)\}$, respectively. The truncation of the time interval is needed as the stationary data theoretically persists forever and thus just the finite-range Fourier transforms exists [3]. We introduce the definition of the Riesz fractional integral $(I^\gamma f)(t)$

$$(I^\gamma f)(t) = \frac{1}{2\nu(\gamma)} \int_{-\infty}^{\infty} \frac{f(\tau)}{|t - \tau|^{1-\gamma}} \mathrm{d}\tau; \qquad Re\gamma > 0, \gamma \neq 1, 3, 5, ... \tag{23}$$

where $\nu(\gamma) = \Gamma(\gamma)\cos(\gamma\pi/2)$. For differentiable functions, it can be shown that the inverse Fourier transform of the Riesz fractional integral $(I^\gamma f)(t)$ from the time in the frequency domain is given by

$$\mathcal{F}^{-1}\{(I^\gamma f)(t); \omega\} = |\omega|^{-\gamma} \mathcal{F}^{-1}\{f(t); \omega\} = |\omega|^{-\gamma} F(\omega) \tag{24}$$

Rewriting Eq.(22) leads to

$$F_k(\omega, T) = \frac{1}{4\pi i} \int_{\rho - i\infty}^{\rho + i\infty} \Pi_H(-\gamma) \mathcal{F}^{-1}\{\left(I^{1-\gamma} W_k\right)(t, T); \omega\} d\gamma \tag{25}$$

Applying a finite Fourier transform finally leads to a reconstruction of the correlated noise process $\{F(t)\}$ in terms of the H-FSMs given by

$$F(t) = \lim_{T \to \infty} E\left[F_k(t, T)\right] = \frac{1}{4\pi i} \int_{\rho - i\infty}^{\rho + i\infty} \Pi_H(-\gamma)(I^{1-\gamma} W)(t) \mathrm{d}\gamma \tag{26}$$

where $E\left[F_k(t, T)\right]$ is the expected value operation over the ensemble index k. In [13] a computational efficient algorithm for the digital simulation of wind loads based on Eq.(26) is introduced.
In the following, this method is used in order to develop a state space representation of the colored load process. Using the approximation of the transfer function $H(\omega)$ given in Eq.(13b), the integral representation of the colored load process defined in Eq.(26) can be approximated by the truncated sum

$$F(t) \approx \frac{\Delta\eta}{4\pi} \sum_{k=-m}^{m} \Pi_H(-\gamma_k)(I^{1-\gamma_k} W)(t) \tag{27}$$

Hence, the main difficulty in the simulation of the process lies in the efficient calculation of the Riesz fractional integral $(I^{1-\gamma_k} W)(t)$ of the Gaussian white noise process $\{W(t)\}$. It can

be shown that the Riesz integral form can be expressed in terms of Riemann-Liouville (RL) fractional integrals

$$(28)\quad (I^{\gamma}W)(t) = \frac{1}{2\nu(\gamma)}\left[\int_{-\infty}^{t}\frac{W(\tau)}{|t-\tau|^{1-\gamma}}d\tau + \int_{t}^{\infty}\frac{W(\tau)}{|\tau-t|^{1-\gamma}}d\tau\right] = \frac{(I_{+}^{\gamma}W)(t)+(I_{-}^{\gamma}W)(t)}{2\cos(\gamma\pi/2)}$$

with $-\infty < t < \infty$ and $\nu(\gamma) = \Gamma(\gamma)\cos(\gamma\pi/2)$ and where $(I_{+}^{\gamma}W)(t)$, $(I_{-}^{\gamma}W)(t)$ denote the left-, right-handed RL fractional integral, respectively [49, p. 214]. Assuming that the process $\{W(t)\}$ is discretized on a finite interval $[0, n\tau]$, where $n \in \mathbb{N}$, $\tau > 0$, and zero elsewhere, the RL integrals can be calculated numerically using fractional order differences as i.e. shown in [49, p. 385–388]. This leads to the Grünwald - Letnikov form of the Riesz fractional integral given by:

$$(29)\qquad (I^{\gamma}W)(j\tau) \approx \lim_{\tau\to+0}\sum_{k=0}^{j}\alpha_k(\gamma)W(j\tau-k\tau) + \lim_{\tau\to+0}\sum_{k=0}^{n-j}\alpha_k(\gamma)W(j\tau+k\tau)$$

where

$$(30)\qquad \alpha_k(\gamma) = \frac{(-1)^k\tau^{\gamma-1}}{2\cos(\gamma\pi/2)}\begin{pmatrix}-\gamma\\ k\end{pmatrix}$$

Eq.(29) can be calculated efficiently in matrix form by $\mathbf{Z}(\gamma) = \mathbf{A}(\gamma)\mathbf{W}$

$$(31)\quad \mathbf{Z}(\gamma) = \begin{bmatrix}(I^{\gamma}W)(0)\\ (I^{\gamma}W)(\tau)\\ \dots\\ (I^{\gamma}W)(n\tau)\end{bmatrix};\quad \mathbf{A}(\gamma) = \begin{bmatrix}2\alpha_0 & \alpha_1 & \dots & \alpha_n\\ \alpha_1 & 2\alpha_0 & \dots & \dots\\ \dots & \dots & \dots & \alpha_1\\ \alpha_n & \dots & \alpha_1 & 2\alpha_0\end{bmatrix};\quad \mathbf{W} = \begin{bmatrix}W(0)\\ W(\tau)\\ \dots\\ W(n\tau)\end{bmatrix} = \begin{bmatrix}G_0\\ G_1\\ \dots\\ G_n\end{bmatrix}$$

where the discretized white noise process $\mathbf{W}$ in the interval $[0, n\tau]$ is described by the realizations of a zero-mean Gaussian random process $G_0, G_1, \dots, G_n$ with standard deviation $\sqrt{q\tau}$. The vector of the colored load process $\mathbf{F} = [F(0), F(\tau), \dots, F(n\tau)]^T$ is finally obtained by

$$(32)\qquad \mathbf{F} = \frac{\Delta\eta}{4\pi}\sum_{k=-m}^{m}\Pi_H(-\gamma_k)\mathbf{Z}(1-\gamma_k) = \sum_{k=-m}^{m}\mathbf{h}(\gamma_k)\mathbf{W}$$

by means of the matrix transfer function $\mathbf{h}(\gamma_k) = \Delta\eta(4\pi)^{-1}\Pi_H(-\gamma_k)\mathbf{A}(1-\gamma_k)$.

2.2.1 Numerical examples

The result in Eq.(32) is once again verified by means of the three load cases. In Fig.(2) (Bottom) the three generated time series and the corresponding AC functions (Top) are depicted. It can be stressed that there is a good agreement between the analytic AC function and the one obtained from the generated time series. The load process are simulated with a time interval $\tau = 0.05$ [s] using the following parameters:

- Exponentially correlated wind gusts: $p = 250$, $m = 30$, $\rho = 0.6$, $\Delta\eta = 0.2$
- Wind gusts with von Kármán velocity PSD: $p = 400$, $m = 50$, $\rho = 0.6$, $\Delta\eta = 0.15$
- Wind waves with P-M PSD: $p = 600$, $m = 100$, $\rho = 1.6$, $\Delta\eta = 0.3$

where p denotes the number of considered $\alpha_k(\gamma)$ coefficients as explained in the next section.

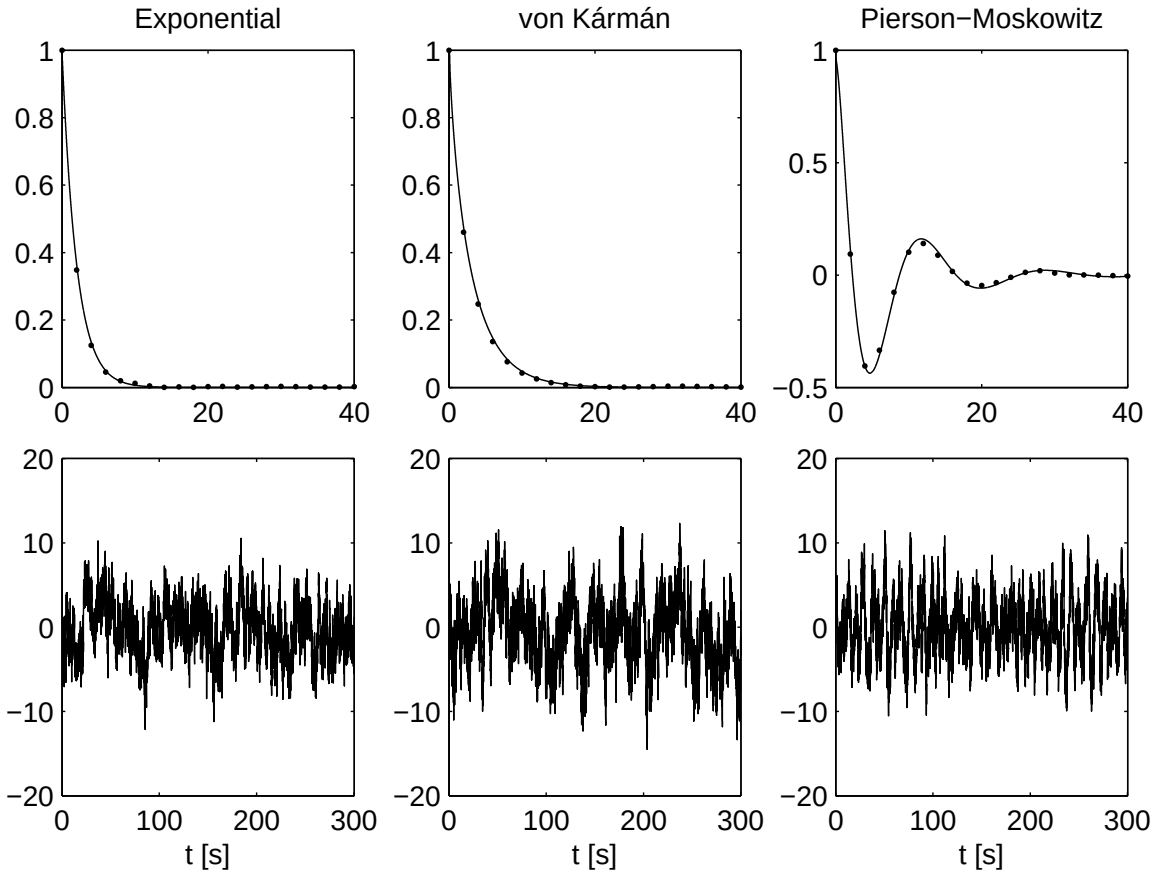

Figure 2: Top: Exact (continuous) and approximated (dotted) normalized AC functions, Bottom: Generated time series for the three load cases: exponential AC, von Kármán and P-M PSD

2.2.2 Generalized state space representation of colored random processes

Based on the result given in Eq.(32) we will now develop a general state space representation for colored load processes. It must be stressed that it is valid for arbitrary correlated Gaussian processes and can be given directly once the H-FSMs in Eq.(11) are calculated.
Due to the Toeplitz form of the coefficient matrix $\mathbf{A}(\gamma)$ the matrix transfer function $\mathbf{h}(\gamma_k)$ in Eq.(32) can be calculated easily. Furthermore, if $Re\gamma > -1$ is chosen, then the coefficients $\alpha_k(\gamma)$ decrease with inverse power law behavior as k increases and can be neglected in this case after a finite number of terms p, which mainly depends on the decay of the correlation function. It must be noted that for an input vector $\mathbf{W}$ of length n, the first and last p samples of the output $\mathbf{F}$ can be regarded as the 'transition states' whereas the remaining $n-2p$ samples are the 'steady states' which are needed in the following for the formulation of a recursive state space form. The calculation of one steady state realization $F_j = F(j\tau)$ of the discrete load process $\mathbf{F}$, with $j = 0, 1, \ldots, n$ is given by

$$F_j = \frac{\Delta\eta}{4\pi} \sum_{k=-m}^{m} \Pi(-\gamma_k) \begin{bmatrix} \alpha_p(1-\gamma_k) \\ \alpha_{p-1}(1-\gamma_k) \\ \cdots \\ 2\alpha_0(1-\gamma_k) \\ \cdots \\ \alpha_{p-1}(1-\gamma_k) \\ \alpha_p(1-\gamma_k) \end{bmatrix}^T \begin{bmatrix} G_{j-p} \\ G_{j-p+1} \\ \cdots \\ G_j \\ \cdots \\ G_{j+p-1} \\ G_{j+p} \end{bmatrix} = \begin{bmatrix} \beta_p \\ \beta_{p-1} \\ \cdots \\ 2\beta_0 \\ \cdots \\ \beta_{p-1} \\ \beta_p \end{bmatrix}^T \begin{bmatrix} G_{j-p} \\ G_{j-p+1} \\ \cdots \\ G_j \\ \cdots \\ G_{j+p-1} \\ G_{j+p} \end{bmatrix} \tag{33}$$

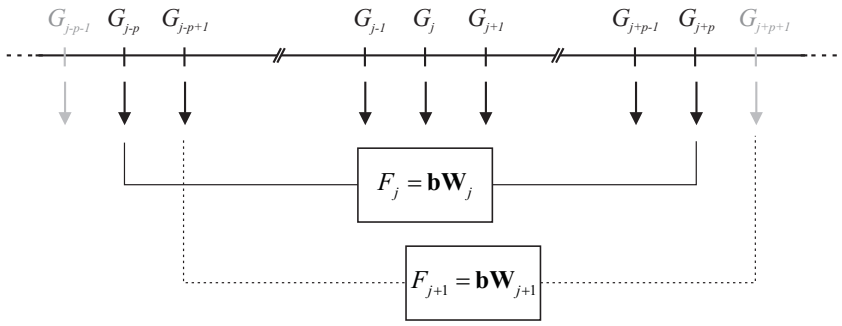

Figure 3: Steady state realization of the load process: the load F_{j+1} of the next time step is generated by shifting the p-dimensional vector $\mathbf{W}_j$ of increments of white noise

where

$$\beta_p = \frac{\Delta\eta}{4\pi} \sum_{k=-m}^{m} \Pi_H(-\gamma_k)\alpha_p(1-\gamma_k) \tag{34}$$

as illustrated in Fig.(3). As one can see from Eq.(33) the actual sample $F_j = \mathbf{bW}_j$ of the load process is calculated by the time-invariant vector $\mathbf{b} = [\beta_p, \beta_{p-1}, ..., 2\beta_0, ..., \beta_{p-1}, \beta_p]$ including the weights of the $(2p+1)$ elements of the vector of the white input noise $\mathbf{W}_j = [G_{j-p}, ..., G_j, ..., G_{j+p}]$ consisting out of the p previous and past samples of the Gaussian noise process. This allows to formulate a recursive state space representation, which is needed later in order to include the colored noise process $\{F(t)\}$ into the Kalman filter algorithm, by a forward shift of the white noise process as shown in Fig.(3). This leads to the following state space form

$$\begin{aligned} \mathbf{x}'_{k+1} &= \mathbf{A}_d\mathbf{x}'_k + \mathbf{B}_d w_k \\ F_k &= \mathbf{C}_d\mathbf{x}'_k \end{aligned} \tag{35}$$

where $\mathbf{x}'_k = [G_{k-p}, G_{k-p+1}, ..., G_k, ..., G_{k+p-1}, G_{k+p}]^T$ and with time-invariant transfer matrices $\mathbf{A}_d$, $\mathbf{B}_d$ and $\mathbf{C}_d$

$$\mathbf{A}_d = \begin{bmatrix} 0 & 1 & 0 & \dots & \dots & 0 & 0 \\ \dots & 0 & 1 & 0 & \dots & \dots & 0 \\ \dots & \dots & 0 & 1 & 0 & \dots & \dots \\ \dots & \dots & \dots & 0 & \cdots & \dots & \dots \\ \dots & \dots & \dots & \dots & \dots & \dots & \dots \\ 0 & \dots & \dots & \dots & \dots & 0 & 1 \\ 0 & 0 & \dots & \dots & \dots & 0 & 0 \end{bmatrix} \quad \mathbf{B}_d = \begin{bmatrix} 0 \\ 0 \\ \dots \\ \dots \\ \dots \\ 0 \\ 1 \end{bmatrix} \quad \mathbf{C}_d = \begin{bmatrix} \beta_p \\ \beta_{p-1} \\ \cdots \\ 2\beta_0 \\ \cdots \\ \beta_{p-1} \\ \beta_p \end{bmatrix}^T \tag{36}$$

In the following the subindex d for discrete-time will be omitted for simplicity of notation. It shall be highlighted that Eq.(35) is a general state space representation of stationary arbitrarily colored load processes with known PSD. Once, the H-FSM of the PSD are determined using Eq.(11) the corresponding state space form is defined by Eq.(35).

3 Kalman filter algorithm for correlated process noise

The Kalman filter (KF) was developed in 1960 by Rudolf Kálmán [30]. It is an optimal recursive algorithm to estimate the state $\mathbf{x} \in \mathbb{R}^n$ of a linear dynamic system discretized in the time domain using noisy measurement data $\mathbf{z} \in \mathbb{R}^m$. The discretized state space model

Time Update (Prediction)	Measurement Update (Correction)
Prior estimate $\bar{\mathbf{x}}_{k+1} = \mathbf{T}\mathbf{x}_k$	Kalman gain matrix Posterior estimate $\mathbf{K}_k = \bar{\Sigma}_{xx,k+1}\mathbf{H}^T(\Sigma_{vv,k} + \mathbf{H}\bar{\Sigma}_{xx,k+1}\mathbf{H}^T)^{-1}$
Prior error covariance: $\bar{\Sigma}_{xx,k+1} = \mathbf{T}\Sigma_{xx,k}\mathbf{T}^T + \mathbf{S}\Sigma_{ww,k}\mathbf{S}^T$	Posterior estimate $\mathbf{x}_{k+1} = \bar{\mathbf{x}}_{k+1} + \mathbf{K}_k(\mathbf{z}_{k+1} - \mathbf{H}\bar{\mathbf{x}}_{k+1})$
	Posterior error covariance $\Sigma_{xx,k+1} = \bar{\Sigma}_{xx,k+1} - \mathbf{K}_k\mathbf{H}\bar{\Sigma}_{xx,k+1}$

Table 1: Kalman filter algorithm

of a system excited by a Gaussian white noise process $\mathbf{w}$ is generated by two equations, the system and measurement equation

$$\begin{aligned} \mathbf{x}_{k+1} &= \mathbf{T}\mathbf{x}_k + \mathbf{S}\mathbf{w}_k \\ \mathbf{z}_k &= \mathbf{H}\mathbf{x}_k + \mathbf{v}_k \end{aligned} \tag{37}$$

where $\mathbf{T} \in \mathbb{R}^{n\times n}$, $\mathbf{S} \in \mathbb{R}^{n\times u}$ and $\mathbf{H} \in \mathbb{R}^{m\times n}$ are the transfer matrices and $\mathbf{w}_k \in \mathbb{R}^u$ and $\mathbf{v}_k \in \mathbb{R}^m$ are uncorrelated stationary zero-mean white noise processes. The transfer matrix $\mathbf{T}$ relates the actual state at time k to the state at the next time step $k+1$. The model uncertainties or unmeasured disturbances are represented by the added m-dimensional noise vector $\mathbf{w}_k$ which is related to the actual state by the matrix $\mathbf{S}$. The KF is based on a Gaussian noise model, i.e. the measurement error $\mathbf{v}_k \sim N(\mathbf{0}, \mathbf{\Sigma}_{vv,k})$ as well as the state error $\mathbf{w}_k \sim N(\mathbf{0}, \mathbf{\Sigma}_{ww,k})$ are modeled as independent, white noises with normal distribution where $\mathbf{\Sigma}_{vv,k} \in \mathbb{R}^{m\times m}$, $\mathbf{\Sigma}_{ww,k} \in \mathbb{R}^{n\times n}$ denotes the measurement and process noise covariance matrix, respectively. The algorithm is characterized by an iterative prediction-correction structure as shown in Tab.(1). In the *prediction step* a time update of the current state $\mathbf{x}_k$ and error covariance matrix $\mathbf{\Sigma}_{xx,k}$ is taken in order to obtain a prior estimate of the process state $\bar{\mathbf{x}}_{k+1}$ and its associated error covariance matrix $\bar{\mathbf{\Sigma}}_{\bar{x}\bar{x},k+1}$ of the next time step. The time-update of the current state is calculated from the undisturbed system equation $\bar{\mathbf{x}}_{k+1} = \mathbf{T}\mathbf{x}_k$ where the prediction error leads to the update of the covariance matrix and where the tilde indicates the true state

$$\begin{aligned} \epsilon_{\bar{x},k+1} &= \tilde{\mathbf{x}}_{k+1} - \bar{\mathbf{x}}_{k+1} = \mathbf{T}(\tilde{\mathbf{x}}_k - \mathbf{x}_k) + \mathbf{S}(\tilde{\mathbf{w}}_k - \mathbf{w}_k) \\ \mathbf{\Sigma}_{\bar{x}\bar{x},k+1} &= E[\epsilon^T_{\bar{x},k+1}\epsilon_{\bar{x},k+1}] = \mathbf{T}\mathbf{\Sigma}_{xx,k}\mathbf{T}^T + \mathbf{S}\mathbf{\Sigma}_{ww,k}\mathbf{S}^T \end{aligned}$$

In the *correction step* the measurement equation is used to predict the likeliest measurement for the given prior state estimate. Once the actual measurement is obtained, the difference $\mathbf{d}_k = \mathbf{H}\bar{\mathbf{x}}_k - \mathbf{z}_k$ between the predicted measurement and the actual measurement, also known as innovation or residual, is calculated. The Kalman gain matrix $\mathbf{K}_k$ is determined in order to correct the prior state estimate $\bar{\mathbf{x}}_{k+1}$ in the measurement update. It is the result of the minimization of the mean-square error of the posterior state estimate $\mathbf{x}_{k+1}$

$$\begin{aligned} \epsilon_{x,k+1} &= \tilde{\mathbf{x}}_{k+1} - \mathbf{x}_{k+1} \\ E[\epsilon^T_{x,k+1}\epsilon_{x,k+1}] &\rightarrow min. \end{aligned} \tag{38}$$

It leads to the Kalman gain matrix $\mathbf{K}_k$ which is used to calculate the optimal estimate $\mathbf{x}_{k+1}$ and its associated posterior error covariance $\mathbf{\Sigma}_{xx,k+1}$ as shown in Tab.(1) [45].

In case that the white noise assumption of the load process w_k in Eq.(37) is violated, the KF equations are no longer valid. However, a modification of the KF algorithm for colored

noises based on the spectral factorization theorem has been proposed in [34]. It allows to relax the white noise assumption and to consider either (i) correlation of measurement and process noise, (ii) autocorrelated measurement noise or (iii) autocorrelated process noise into the model. Here, the latter case is discussed. To this aim, a state space representation of the transfer function $H(\omega)$ in the form

$$\begin{aligned} \dot{\mathbf{x}}(t) &= \mathbf{A}\mathbf{x}(t) + \mathbf{B}w(t) \\ F(t) &= \mathbf{C}\mathbf{x}(t) \end{aligned} \tag{39}$$

must be found where the input $w(t)$ is a Gaussian white noise process and the output $F(t)$ is the sought colored load process with target PSD function. State-space equations such as given in Eq.(39) are non-unique. Among the so-called canonical state space models, the controllable canonical form is given by setting [29]

$$\mathbf{A} = \begin{bmatrix} -b_0 & -b_1 & \dots & \dots & -b_{n-1} \\ 1 & 0 & \dots & 0 & 0 \\ 0 & 1 & \dots & \dots & \dots \\ \dots & \dots & \dots & 0 & 0 \\ 0 & \dots & 0 & 1 & 0 \end{bmatrix} \qquad \mathbf{B} = \begin{bmatrix} 1 \\ 0 \\ \dots \\ \dots \\ 0 \end{bmatrix} \qquad \mathbf{C} = \begin{bmatrix} a_0 \\ a_1 \\ \dots \\ a_{m-1} \\ \dots \\ 0 \end{bmatrix}^T \tag{40}$$

assuming that the state $\mathbf{x}(t) = [x_1(t), x_2(t), \dots, x_n(t)]$ is of order n. The discretization of Eq.(39) finally leads to the linear state space representation

$$\begin{aligned} \mathbf{x}'_{k+1} &= \mathbf{A}_d\mathbf{x}'_k + \mathbf{B}_d w_k \\ F_k &= \mathbf{C}_d\mathbf{x}'_k \end{aligned} \tag{41}$$

which will be used in the following to extend the KF for colored process noise $\{F(t)\}$ with target PSD $S_F(\omega)$. The state space representation of some fundamental stochastic processes such as random bias, first- and second-order Markov process, Brownian motion can be found e.g. in [34]. In [28] the method is applied to introduce a colored process describing the surface roughness of the road into the Kalman filter in order to estimate the states of the vehicle. Comparing Eq.(41) with the state space representation in Eq.(35) obtained in the previous section by H-FSMs decomposition, the strong resemblance of these two representations is obvious.

3.1 Modification of the Kalman Filter

Following the approach given in [34] the Kalman filter is extended for colored process noise with given PSD by passing a white noise w_k through a linear filter. Augmenting the state vector $\mathbf{x}_{a,k} = [\mathbf{x}_k, \mathbf{x}'_k]^T$ where $\mathbf{x}_k$ are the states of the system and $\mathbf{x}'_k$ represents additional states related to the state space representation of the transfer function $H(\omega)$ of the load process derived either by spectral factorization (41) or by H-FSMs decomposition (35), leads to a state space model

$$\begin{aligned} \begin{bmatrix} \mathbf{x}_{k+1} \\ \mathbf{x}'_{k+1} \end{bmatrix} &= \begin{bmatrix} \mathbf{T}_d & \mathbf{S}_d\mathbf{C}_d \\ \mathbf{0} & \mathbf{A}'_d \end{bmatrix} \begin{bmatrix} \mathbf{x}_k \\ \mathbf{x}'_k \end{bmatrix} + \begin{bmatrix} \mathbf{0} \\ \mathbf{B}_d \end{bmatrix} w_k \\ \mathbf{z}_{a,k} &= \begin{bmatrix} \mathbf{H}_d & \mathbf{0} \end{bmatrix} \begin{bmatrix} \mathbf{x}_k \\ \mathbf{x}'_k \end{bmatrix} + \begin{bmatrix} \mathbf{v}_k \\ \mathbf{0} \end{bmatrix} \end{aligned} \tag{42}$$

which is once again a linear system excited by white noise. Hence, after rewriting Eq.(42)

$$\begin{aligned} \mathbf{x}_{a,k+1} &= \mathbf{T}_a\mathbf{x}_{a,k} + \mathbf{S}_a\mathbf{w}_k \\ \mathbf{z}_{a,k} &= \mathbf{H}_a\mathbf{x}_{a,k} + \mathbf{v}_{a,k} \end{aligned} \tag{43}$$

the KF algorithm given in Tab.(1) can be run on the augmented state space model (42) using the modified transfer matrices $\mathbf{T}_a$, $\mathbf{S}_a$ and $\mathbf{H}_a$, respectively.
In order to apply the method for identification problems a further modification is needed in order to estimate the unknown parameters. Following the approach of the extended Kalman filter (EKF), the state $\mathbf{x}_{a,k}$ has to be augmented to include the model parameters $\mathbf{p}_k$ leading to a nonlinear system equation of the extended state $\mathbf{x}_{ext,k} = [\mathbf{x}_{a,k}, \mathbf{p}_k]^T$

$$\begin{aligned} \mathbf{x}_{ext,k+1} &= f(\mathbf{x}_{ext,k}) + \mathbf{S}_{ext}\mathbf{w}_{ext,k} \\ \mathbf{z}_{ext,k} &= h(\mathbf{x}_{ext,k}) + \mathbf{v}_{ext,k} \end{aligned} \tag{44}$$

as the system matrices $\mathbf{T}_a$, $\mathbf{H}_a$ depend nonlinearly on the estimates of the state $\mathbf{x}_{a,k}$ and the parameters $\mathbf{p}_k$ known from the previous time step. In case of weak nonlinearities the identification problem is solved using the EKF which linearizes about the current mean and covariance by applying a first order Taylor expansion of Eq.(44) near the current state estimate leading to the time variant extended system matrices $\mathbf{T}_{ext,k}$, $\mathbf{H}_{ext,k}$

$$\begin{aligned} \mathbf{T}_{ext,k} &= \frac{\partial f(\mathbf{x}_{ext,k})}{\partial x_{ext,k}} \\ \mathbf{H}_{ext,k} &= \frac{\partial h(\mathbf{x}_{ext,k})}{\partial x_{ext,k}} \end{aligned} \tag{45}$$

to be calculated at each time step.

The standard KF algorithm shown in Tab.(1) can be now run on the linearized model: first the prior estimate is calculated by the nonlinear state space model given in Eq.(44), then the update of the error covariances and the measurement update is calculated by introducing the extended system matrices.

4 Numerical application

The proposed method is now applied to a single degree of freedom (SDOF) system excited by the introduced three load cases in order to estimate the stiffness and damping parameter.

1. Exponentially correlated wind gusts:
The first example is taken from [34] and is used in order to show the consistency of the introduced algorithm based on the H-FSMs decomposition and the factorization method introduced there. In this example the (long period) longitudinal dynamics of an aircraft are approximated by the continuous state space model of a harmonic oscillator with natural eigenfrequency $\omega = \sqrt{k/m}$ and ratio of critically damping $D = c/(2m\omega)^{-1}$ given by

$$\dot{\mathbf{x}} = \begin{bmatrix} 0 & 1 \\ -\omega^2 & -2D\omega \end{bmatrix} \mathbf{x} + \begin{bmatrix} 0 \\ 1/m \end{bmatrix} w_c \tag{46}$$

where $\mathbf{x} = [\phi, \dot{\phi}]^T$ and ϕ denotes the pitch angle, i.e. the angle between the longitudinal axis of the aircraft and the horizon. The colored process noise w_c represents wind gusts with exponential AC function $R(\tau) = \sigma^2 e^{-a|t|}$. Performing the spectral factorization on the corresponding PSD in Eq.(14) results in the so-called shaping filter $H(s)$, that is the Laplace transform counterpart of the transfer function $H(\omega)$, of the noise $w_c(t)$ in the form

$$H(s) = \frac{\sigma}{a + s} \tag{47}$$

Further details on the spectral factorization can be found in [34, 36]. Using the controllable canonical state space representation in Eq.(40), the shaping filter $H(s)$, given in Eq.(47) corresponds in the time domain to the first order Markov model

$$\dot{x}' = -ax' + w' \qquad w_c = x' \tag{48}$$

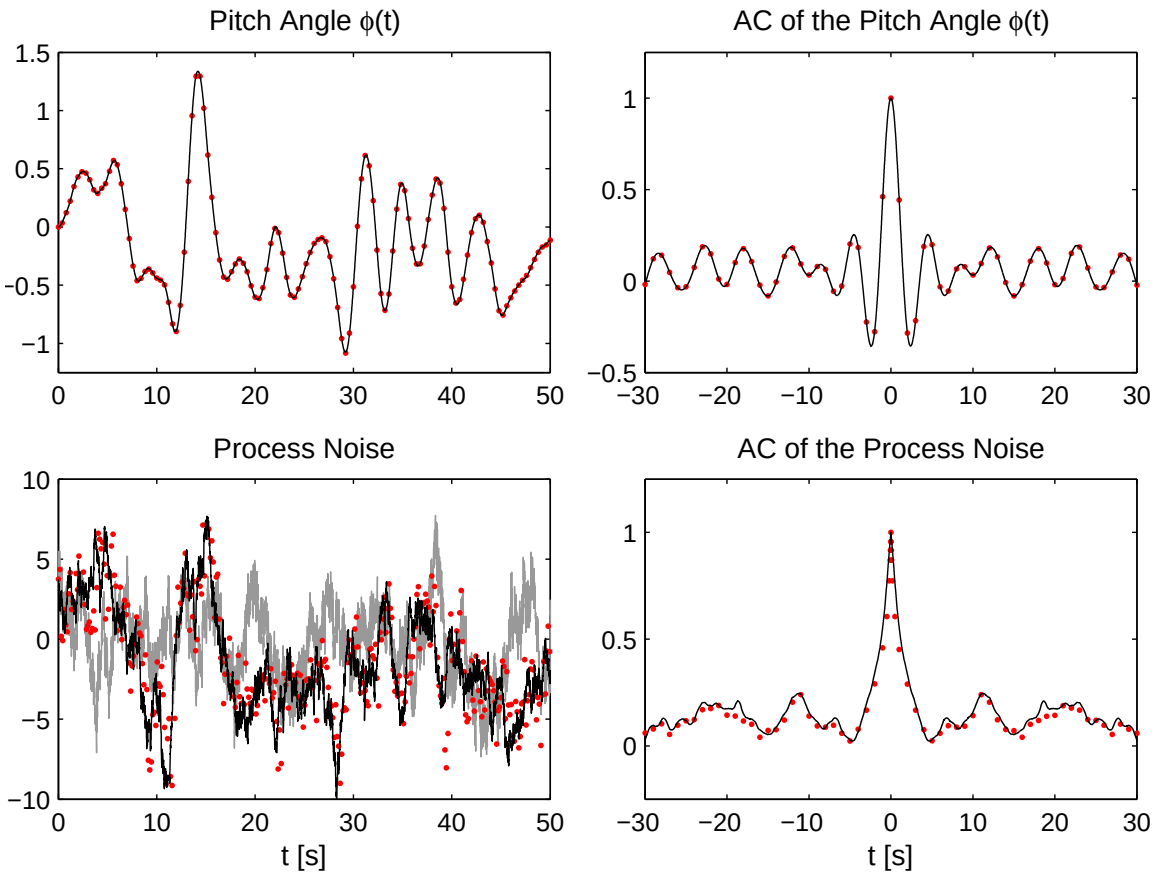

Figure 4: Top: Evaluation of the pitch angle $\phi(t)$ for $\omega = \sqrt{2}$ [rad/s], $D = 0.05$ [-], Bottom: Colored process noise generated by spectral factorization (black), by H-FSMs (gray) and estimated by the fractional KF (red dotted)

which is excited by a Gaussian white noise w' with standard deviation σ. It is used in order to augment the state space model in Eq.(46) leading to

$$\dot{\mathbf{x}}_a = \begin{bmatrix} 0 & 1 & 0 \\ -\omega^2 & -2D\omega & 1/m \\ 0 & 0 & -a \end{bmatrix} \mathbf{x}_a + \begin{bmatrix} 0 \\ 0 \\ 1 \end{bmatrix} w' \tag{49}$$

where $\mathbf{x}_a = [\phi, \dot{\phi}, x']^T$ denote the augmented state. After discretization of the augmented model, e.g. by Euler approximation or by using the matrix exponential function, a linear model excited by Gaussian white noise in the form of Eq.(43) is obtained. It will be used in this example for the generation of the 'true' measurement of the pitch angle $\phi(t)$ used in the KF algorithm.

By means of the approach using fractional calculus the augmented state space model is obtained by the following procedure: (i) the system's state space representation is formulated, (ii) the H-FSMs are calculated from the target PSD and the weights β_k of the Gaussian white noise are determined using Eq.(34), (iii) the initial vector $\mathbf{x}'_0$ of increments of Gaussian white noise and the system matrices of the generalized state space model in Eq.(35) are stored and introduced in Eq.(42) to obtain the augmented state space model. In the following, the KF algorithm based on this approach will be indicated as 'H-fractional KF' and the corresponding noise is denoted as 'H-fractional noise', respectively.

The evaluation of the pitch angel and the input force is estimated from output-only measurements using the H-fractional KF. Fig.(4) depicts the evaluation and AC of the pitch angle $\phi(t)$

case	in. value		id. par.		st. dev.		id. err.	
	$\hat{k_0}$	$\hat{c_0}$	$\hat{k}$	$\hat{c}$	$\sigma_{\hat{k}}$	$\sigma_{\hat{c}}$	ϵ_k	ϵ_c
Exponential	5	0.35	9.93	0.79	0.15	0.12	0.7	11.7
von Karman	5	0.35	10.01	0.82	0.28	0.18	0.1	16.2
Pierson Moskowitz	5	0.35	9.96	0.81	0.20	0.18	0.4	14.6
true values	$k = 10$ N/m, $c = 0.707$ Ns/m							

Table 2: Identification results for the different load cases. $\hat{k}_0$ in [N/m] and $\hat{c}_0$ in [Ns/m] are the initial estimate, $\hat{k}$ and $\hat{c}$ are the identified parameters, σ_k in [N/m], σ_c in [Ns/m] and ϵ in [%] are the standard deviation and the identification error, respectively.

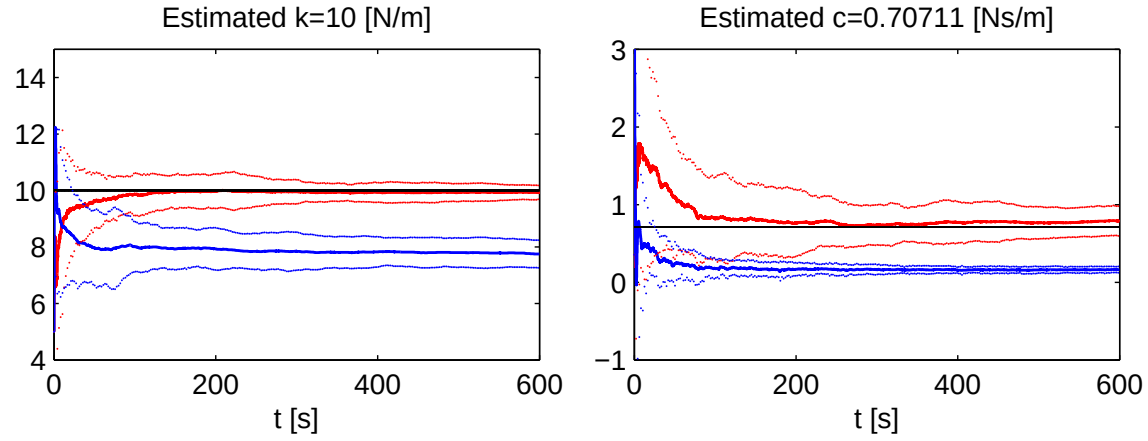

Figure 5: Estimation of the stiffness k [N/m] and damping constant c [Ns/m] of the SDOF system excited by an exponentially correlated load process by means of H-fractional EKF (red) and the standard EKF (blue). The dotted lines represent the corresponding 90 % confidence intervals.

(Top) and the corresponding process noise exciting the system (Bottom). In order to illustrate that the KF algorithm not just updates the pitch angle $\phi(t)$ but also the H-fractional noise, the load process is depicted in gray for the case without consideration of the measurement date and in red after applying the KF algorithm.

In order to estimate the system's stiffness $k = 10$ [N/m] and damping constant $c = 0.707$ [Nm/s] ($D = 0.05$) now the so-called 'H-fractional EKF' is applied. The state space model of the H-fractional EKF are obtained by augmenting the state representation of the H-fractional Kalman filter by the stiffness and damping parameter. The resulting nonlinear system equations given in Eq.(44) are then linearized with respect to the actual state estimate using Eq.(45). It is assumed that noisy measurement date of the pitch angle $\phi(t)$ and the velocity $\dot{\phi}(t)$ is available taking into account a measurement error of $\sigma_z = 1$ [cm] which corresponds to 1 % of the maximal deflections. It is assumed that a set of 20 measurements of a duration of 10 [min.] each are available. The H-fractional EKF as well as the standard EKF are run on the samples. In the latter case the correlation of the load process is neglected and modeled as white noise with equivalent standard deviation. The initial values of the stiffness and damping parameter $\hat{k}_0$, $\hat{c}_0$ are selected considering an estimation error $\epsilon_{k_0} = |\hat{k}_0 - k|/k$, $\epsilon_{c_0} = |\hat{c}_0 - c|/c$ of 50% of the true values. The mean value as well as the corresponding 90% confidence intervals of the identified model parameters are depicted in Fig.(5).

In case of the H-fractional EKF, the stiffness parameter is estimated with high accuracy while the identification of the damping parameter leads to an error of 11.7 %. As the damping parameter of weakly damped systems has no significant effect on the modal frequencies

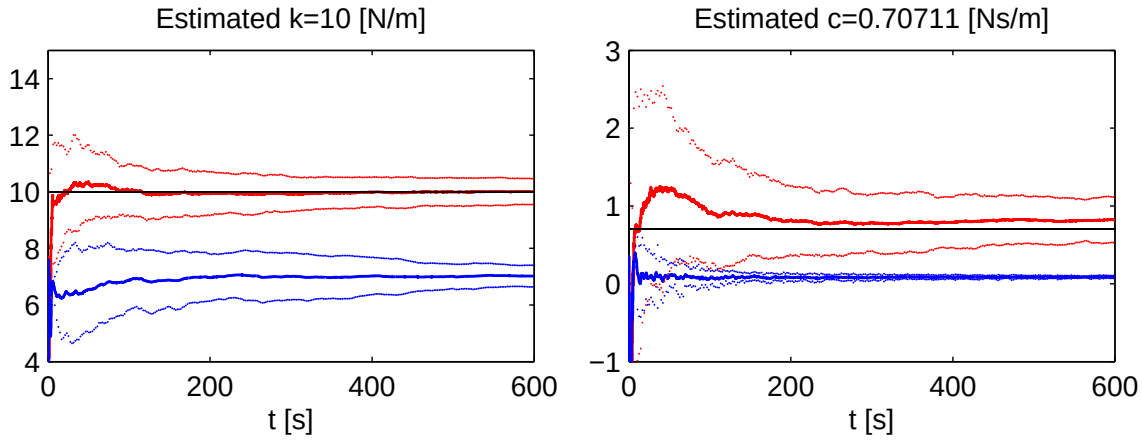

Figure 6: Estimation of the stiffness k [N/m] and damping constant c [Ns/m] of the SDOF system excited by wind loads with von Kármán velocity PSD by means of H-fractional EKF (red) and the standard EKF (blue). The dotted lines represent the corresponding 90 % confidence intervals.

and the observed system response of naturally excited systems, the accuracy of the damping estimation is not very high and even in numerical simulations errors of about 20 % are not unusual [7]. Neglecting the correlation of the load process leads to poor identification results as shown by means of the standard EKF which fails to identify both the stiffness and damping parameter. The results of the parameter identification of the H-fractional EKF are summarized in Tab.(2).

2. Wind gusts with von Kármán velocity PSD
As shown in section 2.1.1 the corresponding H-FSMs are different, but the implementation of the filter is the same as in the previous example. The results of the parameter identification for the H-Fractional EKF and the standard EKF are illustrated in Fig.(6). Once again the standard EKF leads to poor identification results while the introduced method allows to estimate the stiffness parameter with high and the damping parameter with satisfying accuracy.

3. Wind waves with Pierson-Moskowitz PSD
The results of the parameter identification are shown in Fig.(7). The estimated stiffness and damping parameter correspond to the generalized quantities of the first eigenmode of a clamped vertical pile which is excited by wind-induced ocean waves. The accuracy of the parameter identification is comparable to the previous examples and the results are summarized in Tab.(2). The uncertainties in the damping estimation obtained by the H-fractional EKF are reflected in the high standard deviation σ_c of the damping estimate which leads in all three cases to a relative wide 90% confidence interval. In contrast, the confidence intervals of the damping estimates obtained by the standard EKF are narrow and thus do not comply with the actual quality of the identification results.

5 Conclusions

In this paper we introduced the H-fractional extended Kalman filter for the treatment of arbitrarily autocorrelated load processes in the scope of parameter identification problems. The system's input was represented as output of a fractional differential equation with white noise as input. In contrast to other techniques, such as the spectral factorization method or ARMA models, the coefficients for the noise simulation are calculated in analytical form from the fractional spectral moments of the linear transfer function. Three load cases of engineering

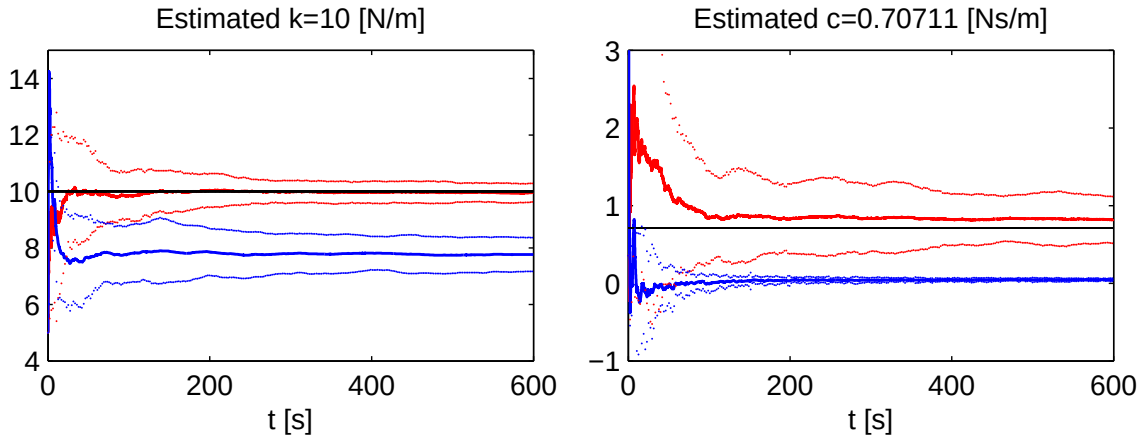

Figure 7: Estimation of the stiffness k [N/m] and damping constant c [Ns/m] of the SDOF system excited by wind loads with P-M PSD by means of H-fractional EKF (red) and the standard EKF (blue). The dotted lines represent the corresponding 90 % confidence intervals.

interest have been studied: a process with (i) exponential autocorrelation function and (ii) von Kármán power spectral density, which are extensively used in wind engineering in order to model along wind turbulences, and (iii) with Pierson Moskowitz power spectral density which is widely used in coastal engineering applications for the description of wind induced waves. In all three cases, we succeeded to give the coefficients for the generation of the load processes in analytical form. Furthermore, a generalized state space representation for colored processes have been developed, which can be given immediately, once the H-fractional spectral moments of the transfer function are calculated. Augmenting the state space model of the excited system by the linear model corresponding to the load process, results in an overall linear system driven by white noise once again to which the extended Kalman filter, a commonly used algorithm for recursive parameter identification, can be applied. This method, indicated as H-fractional extended Kalman filter algorithm, is applied to a SDOF system excited by the three load cases in order to estimate the stiffness and damping parameter using noisy measurement data of the system response. In all examples the stiffness parameter was estimated with high accuracy and the damping parameter was identified with satisfying accuracy. Most output-only identification techniques represent the systems's input as white noise process. In order to illustrate the effect of such a rough simplification if the white noise assumption is violated, the method was compared with the standard extended Kalman filter. It has been shown that neglecting the autocorrelation of the load process leads to poor identification results for both the stiffness and the damping parameter.

Summing up the relevant properties of the method are that: i) it is applicable for arbitrarily correlated loads, i.e. without any restriction to the functional form of the PSD and it is efficient also in case of long-memory processes; ii) the coefficients of the model for the process are known in analytical form and their number can be arbitrarily increased to achieve higher accuracy without recalculation; iii) it is efficiently combined to the Extended Kalman filter; iv) it is easily extendible to multivariate loads, see [10, 13].

References

[1] Arunabha Bagchi. Rational approximations of the power spectral density of atmospheric turbulence arising in adaptive optics. Technical report, University of Twente, 2003.

[2] Julius S. Bendat and Allan G. Piersol. *Engineering Applications of Correlation and Spectral Analysis*. Wiley Series in Probability and Statistics. John Wiley & Sons, 1993.

[3] Julius S. Bendat and Allan G. Piersol. *Random Data - Analysis and Measurement Procedures*. Wiley Series in Probability and Statistics. John Wiley & Sons, 2010.

[4] George E. P. Box, Gwilym M. Jenkins, and Gregory C. Reinsel. *Time Series Analysis: Forecasting and Control*, volume 3 of *Wiley Series in Probability and*. John Wiley & Sons, 2008.

[5] Piet M. T. Broersen and Stijn De Waele. Generating data with prescribed power spectral density. *IEEE Transactions on Instrumentation and Measurement*, 52(4):1061–1067, 2003.

[6] J. M. W. Brownjohn. Ambient vibration studies for system identification of tall buildings. *Earthquake Engineering and Structural Dynamics*, 32:71–95, 2003.

[7] R. Ceravolo. Use of instantaneous estimators for the evaluation of structural damping. *Journal of Sound and Vibration*, 274:385–401, 2004.

[8] Ngai Hang Chan and Wilfredo Palma. State space modeling of long-memory processes. *Annals of Statistics*, 40(1):719–740, 1998.

[9] X. Chen and A. Kareem. Aeroelastic analysis of bridges under multicorrelated winds: Integrated state-space approach. *Journal of Engineering Mechanics*, 127(11):1124–1134, 2001.

[10] Giulio Cottone, Giorgio Barone, and Yukio Tamura. Wind loads spectrum generation by the 'h-fractional spectral moments' decomposition. In *Proceedings of the 13th International Conference on Wind Engineering*, July 2011.

[11] Giulio Cottone and M. Di Paola. A new representation of power spectral density and correlation function by means of fractional spectral moments. *Probabilistic Engineering Mechanics*, 25(3):348–353, 2010.

[12] Giulio Cottone and Mario Di Paola. On the use of fractional calculus for the probabilistic characterization of random variables. *Probabilistic Engineering Mechanics*, 24:321–330, 2010.

[13] Giulio Cottone and Mario Di Paola. Fractional spectral moments for digital simulation of multivariate wind velocity fields. *Journal of Wind Engineering and Industrial Aerodynamics*, 99(6-7):741–747, 2011.

[14] Giulio Cottone, Mario Di Paola, and Ralf Metzler. Fractional calculus approach to the statistical characterization of random variables and vectors. *Physica A*, 389:909–920, 2010.

[15] Giulio Cottone, Mario Di Paola, and Roberta Santoro. A novel exact representation of stationary colored gaussian processes (fractional differential approach). *Journal of Physics A: Mathematical and Theoretical*, 43(085002):16–32, 2010.

[16] Álvaro Cunha and Elsa Caetano. Experimental modal analysis. *Sound and Vibrations*, 40(6):12–20, 2006.

[17] Guido De Roeck, Bart Peeters, and Wei-Xin Ren. Benchmark study on system identification through ambient vibration measurements. In *Proceedings 18th Int. Modal Analysis Conference, San Antonio*, pages 1106–1112, 2000.

[18] Christof Devriendt and Patrick Guillaume. Identification of modal parameters from transmissibility measurements. *Journal of Sound and Vibration*, 314(1-2):343–356, 2008.

[19] Christof Devriendt, Patrick Guillaume, Edwin Reynders, and Guido De Roeck. Operational modal analysis of a bridge using transmissibility measurements. In *Proceedings of the IMAC-XXV*, 2007.

[20] Scott W. Doebling and Charles R. Farrar. Computation of structural flexibility for bridge health moitoring using ambient modal data. In *Proceedings of the 11th ASCE Engineering Mechanics Conference*, pages 1114–1117, 1996.

[21] Youcef Ferdi, Abdelmalik Taleb-Ahmed, and Mohamed Reda Lakehal. Efficient generation of $1/f^{\beta}$ noise using signal modeling techniques. *IEEE Transactions on circuits and systems - 1: Regular papers*, 55(6):1704–1710, 2008.

[22] C. Gentile and A. Saisi. Ambient vibration testing of historic masonry towers for structural identification and damage assessment. *Construction and Building Materials*, 21:1311–1321, 2007.

[23] C. W. J. Granger and Roselyne Joyeux. An introduction to long-memory time series models and fractional differencing. *Journal of Time Series Analysis*, 1(1):15–29, 1980.

[24] D. D. Holm. Taylor′s hypothesis, hamilton′s principle and the LANS-alpha model for computing turbulence. *Los Alamos Science*, 29:172–180, 2005.

[25] Sanja S. Ivanovic, Mihailo D. Trifunac, and Todorovska Maria I. Ambient vibration tests of structures: A review. *ISET Journal of Earthquake Technology*, 37(4):165–197, December 2000.

[26] Bijaya Jaishi and Wei-Xin Ren. Structural finite element model updating using ambient vibration test results. *Journal of Structural Engineering*, ASCE 131(4):617–628, 2005.

[27] George H. James, Thomas G. Carne, and James P. Lauffer. The natural excitation technique (NExT) for modal parameter extraction from operating wind turbines. Technical report, Sandia National Laboratories, 1993.

[28] Weuibong Jeong, Kazuo Yoshida, Hiroki Kobayashi, and Kazuya Oda. State estimation of road surface and vehicle system using a kalman filter. *JSME International Journal*, 33(4):528–534, 1990.

[29] Thomas Kailath. *Linear systems*. Prentice-Hall information and system sciences series. Prentice-Hall, 1980.

[30] Rudolf E. Kálmán. A new approach to linear filtering and prediction problems. *Journal of Basic Engineering*, pages 35–45, 1960.

[31] Holdger Kantz and Thomas Schreiber. *Nonlinear Time Series Analysis*, volume 84 of *Cambridge Nonlinear Science Series 7*. Cambridge University Press, 2008.

[32] Ahsan Kareem. Numerical simulation of wind effects: A probabilistic perspective. *Journal of Wind engineering and Industrial Aerodynamics*, 96:1472–1497, 2008.

[33] J. W. Lee, J. D. Kim, C. B. Yun, and J. M. Shim. Health-monitoring method for bridges under ordinary traffic loadings. *Journal of Sound and Vibration*, 257(2):247–264, 2002.

[34] Frank L. Lewis, Lihua Xie, and Dan Popa. *Optimal and Robust Estimation: With an Introduction to Stochastic Control Theory*. Taylor &Francis Group, 2008.

[35] Jie Li and Jianbing Chen. *Stochastic dynamics of structures*. Wiley, 2009.

[36] Peter S. Maybeck. *Stochastic models, estimation, and control*, volume 1 of *Mathematics in Science and Engineering*. Academic Press, 1979.

[37] Marc P. Mignolet and Pol D. Spanos. Autoregressive spectral modeling: Difficulties and remedies. *International Journal of Non-Linear Mechanics*, 26(6):911 – 930, 1991.

[38] Marcus P. Mignolet and Pol D. Spanos. Recursive simulation of stationary multivariate random processes - part 1. *Journal of Applied Mechanics, ASME*, 109:674–680, 1987.

[39] E. J. Norton and D. C. Quarton. Recommendations for design of offshore wind tubines (RECOFF). Technical report, Garrad Hassan and Partners Ltd, 2003.

[40] Bart Peeters, Guido De Roeck, Luc Hermans, Tom Wauters, Christoph Krämer, and Camiel De Smet. Comparison of system identification methods using operational data of a bridge test. In *Proceedings of ISMA 23, International Conference on Noise and Vibration Engineering*, pages 923–930, Leuven, Belgium, 1998.

[41] Bart Peeters, Guido De Roeck, T. Pollet, and L. Schueremans. Stochastic subspace techniques applied to parameter identification of civil engineering structures. In *Proceedings of New Advances in Modal Synthesis of Large Structures: Nonlinear, Damped and Nondeterministic Cases*, pages 151–162, September 1995.

[42] Bart Peeters, Johan Maeck, and Guido De Roeck. Vibration-based damage detection in civil engineering: excitation sources and temperature effects. *Smart Materials and Structures*, 10:518–527, 2001.

[43] M. Prevesto, M. Olagnon, A. Benveniste, M. Basseville, and G. Le Vey. State space formulation: a solution to modal parameter estimation. *Journal of Sound and Vibration*, 148(2):329–342, 1991.

[44] Wei-Xin Ren and Zhou-Hong Zong. Output-only modal parameter identification of civil engineering structures. *Structural Engineering and Mechanics*, 17(3-4):429–444, 2004.

[45] Katrin Runtemund and Gerhard Müller. Bayesian approach of the skewed Kalman filter applied to an elastically supported structure. In *Proceedings of ISMA, International Conference on Noise and Vibration Engineering, Leuven*, 2010.

[46] Hans Ruscheweyh. *Dynamische Windwirkung an Bauwerken - Band 1: Grundlagen*. Bauverlag, 1982.

[47] Hans Ruscheweyh. *Dynamische Windwirkung an Bauwerken - Band 2: Praktische Anwendungen*. Bauverlag, 1982.

[48] Elias Samaras, Masanobu Shinzuka, and Akira Tsurui. Arma representation of random processes. *Journal of Engineering Mechanics*, 111(3):449–461, 1985.

[49] S.G. Samko, A.A. Kilbas, and O.I. Marichev. *Fractional integrals and derivatives: theory and applications*. Gordon and Breach Science Publishers, 1993.

[50] Masanobu Shinozuka and C.-M. Jan. Digital simulation of random processes and its applications. *Journal of Sound and Vibration*, 25(1):111 – 128, 1972.

[51] Pol D. Spanos. ARMA algorithms for ocean wave modeling. *Journal of Energy Resources Technology*, 105(3):300–309, 1983.

[52] Pol D. Spanos and Marc P. Mignolet. Z-transform modeling of p-wave spectrum. *Journal of Engineering Mechanics*, 112(8):745–759, 1986.

[53] Pol D. Spanos and Marc P. Mignolet. Simulation of stationary random processes: Two stage MA to ARMA approach. *Journal of Engineering Mechanics*, 116(3):620–641, 1990.

[54] Pol D. Spanos and Marcus P. Mignolet. Recursive simulation of stationary multivariate random processes - part 2. *Journal of Applied Mechanics, ASME*, 54:681–687, 1987.

[55] Pol D. Spanos and B. A. Zeldin. Efficient iterative ARMA approximation of multivariate random processes for structural dynamics applications. *Earthquake Engineering & Structural Dynamics*, 25(5):497–507, 1996.

[56] Erik Vanmarcke. *Random fields: analysis and synthesis*. World Scientific, 2010.

[57] Yang. Simulation of random envelope processes. *Journal of Sound and Vibration*, 21(1):73 – 85, 1972.

[58] Ka-Veng Yuen and Lambos S. Katafygiotis. Bayesian time-domain approach for modal updating using ambient data. *Probabilistic Engineering Mechanics*, 16(3):219–231, 2001.